ARTICLE

Probing NaCl hydrate formation from aqueous solutions by Terahertz Time-Domain Spectroscopy

Received 23rd March 2020,
Accepted 13th June 2020

DOI: 10.1039/d0cp01571g

rsc.li/pccp

Ligang Chen,†[a,b,c] Guanhua Ren,†[a,b,c] Liyuan Liu,[a]* Pan Guo,[c] Endong Wang,[c] Zhongjie Zhu,[c] Jinrong Yang,[c] Jianxiong Shen,[b] Zongchang Zhang,[b] Lu Zhou,[a] Jianbing Zhang,[bc] Bin Yang,[d] Weili Zhang,[ae] Yi Gao,[bc] Hongwei Zhao,[bc]* and Jiaguang Han[a]*

The cooling-induced formation of hydrate in aqueous NaCl solutions was probed using terahertz time-domain spectroscopy (THz-TDS). It was found that the NaCl hydrate formation is accompanied with emergence of four new absorption peaks at 1.60, 2.43, 3.34 and 3.78 THz. Combining the X-ray diffraction measurement with the solid-state based density functional theory (DFT) calculations, we assign the observed terahertz absorption peaks to the vibrational modes of the formed $NaCl{\cdot}2H_2O$ hydrate during cooling. This work dedicates THz-TDS based analysis great potential in studying ionic hydrate and the newly revealed collective vibrational modes could be the sensitive indicators to achieve quantitative analysis in phase transitions and lattice dynamics.

Introduction

There is no doubt about the importance of sodium chloride (NaCl) and water interactions that occur in many biological, medical, geological and chemical processes. For example, in the solution environments, the hydrated Na^+ and Cl^- plays a pivotal role in cell membrane transport,[1] acid-base equilibration[2] and charge transport in electrolytes.[3,4] However, With the temperature decrease, solvated Na^+, Cl^- ions and water molecules may form the well-known NaCl hydrates. Such a hydrate formation process often takes place in many cases, such as deicing of roads,[5] and the freezing of cells.[6] Studies on the NaCl hydrate formation are essential for understanding of many biological and chemical processes intrinsically.

Many experimental techniques are developed to investigate the interaction between NaCl and water in various solutions. For example, X-ray diffraction (XRD)[7,8] and neutron diffraction[9,10] were utilized to characterize the structural details of the NaCl hydration shell in aqueous solution. Nuclear magnetic resonance (NMR) spectroscopy was used to discover a liquid-like phase hydration state in quasi-brine layer of dilute NaCl aqueous solution below the liquid-to-solid transition temperature.[11,12] Similarly, these techniques were also used to characterize the structure of solid hydrates.[13,14] Raman spectroscopy was employed to monitor the O-H stretching vibrations of water molecules in NaCl hydrates in both of liquid and frozen phases.[5,15,16] Sum frequency generation spectroscopy (SFG) was also used to probe the dynamics of nucleation and vibrations during freezing NaCl solutions on solid surfaces.[17-19] These techniques provide structural and dynamic information on NaCl hydrate.

Besides, the late-developed terahertz spectroscopy is recently used to study the low-frequency collective vibrations of salt hydration, since terahertz energy is highly sensitive to the changes of molecular conformations and structure.[20,21] In 2010, Bakker *et al.* studied the properties of NaCl hydration shell by monitoring the dynamics of vibrational modes of hydrating water molecules using the combination of terahertz dielectric relaxation (DR) spectroscopy and polarization-resolved femtosecond infrared (IR) spectroscopy.[22] Combing experimental and theoretical terahertz difference spectra, Havenith and Marx *et al.* proved that terahertz spectroscopy could provide an unprecedented view on the details of hydration dynamics. Meanwhile, their result provide clear evidence that the second solvation shell cannot be neglected to describe the terahertz response of cations and anions in water.[23,24] In 2019, Havenith *et al.* studied the strongly rattling modes inside the hydration cages and vibrational fluctuation in the weak hydrating ions.[25] Jepsen *et al.* has utilized terahertz time-domain spectroscopy (THz-TDS) to elucidate the water structural changes in the ionic hydration by characterizing complex dielectric properties of the aqueous NaCl solution. While, there was few molecular fingerprints appeared in the

[a.] *Center for Terahertz Waves and College of Precision Instrument and Optoelectronics Engineering, Tianjin University, Tianjin 300072, People's Republic of China. E-mail: lyliuma@tju.edu.cn; jiaghan@tju.edu.cn*
[b.] *Shanghai Advanced Research Institute Zhangjiang Lab, Chinese Academy of Sciences, Shanghai 201210, China. E-mail: zhaohongwei@sinap.ac.cn*
[c.] *Division of Interfacial Water and Key Laboratory of Interfacial Physics and Technology, Shanghai Institute of Applied Physics, Chinese Academy of Sciences, Shanghai 201800, China.*
[d.] *Faculty of Science and Engineering, University of Chester, Thornton Science Park, Chester, UK, CH2 4NU*
[e.] *School of Electrical and Computer Engineering, Oklahoma State University, Stillwater, Oklahoma 74078, USA*
† These authors contributed equally to this work.
‡ Electronic Supplementary Information (ESI) available. See DOI: 10.1039/x0xx00000x

terahertz regime (0.3-3 THz) due to the spectra broadening effect in the aqueous environment.[26]

It is known that the formation of the hydrated salt is normally accompanied with formation of hydration cage, and the frequency collective motion of the cage, the "rattling", can be probed using terahertz spectroscopy.[25,27-29] Therefore, terahertz spectroscopy provides us the unique fingerprint response to explore the NaCl hydrate formation process. In 2018, Ajito *et al.* has observed two absorption peaks at 1.6 and 2.4 THz risen in NaCl hydrates in dehydration process using freezing-drying, and these resonances were assigned to two types of metastable unit-cell-sized NaCl particles.[30,31] Here, we explored the whole NaCl hydrates formation process from aqueous solutions by using THz-TDS. The measured temperature- and concentration- dependent terahertz spectra not only recorded the phase transition process of the NaCl-H_2O system, but also clearly characterized the formation of the NaCl hydrate from aqueous solutions with newly emerged terahertz absorption peaks. By combining the low-temperature X-ray diffraction and quantum chemical calculations, we also demonstrated that the observed terahertz absorption peaks are well ascribed to the formed NaCl·$2H_2O$ hydrate.

Materials and Methods

Chemicals

NaCl (99.99%, Aldrich Co.) was used without further purification. The distilled water was obtained from a Millipore filtration system with a resistivity of 18.2 MΩ·cm. Eight NaCl solutions were prepared within a broad concentration range from 0 to 4.6 mol/L (M). KCl (99%, Aladdin Industrial Inc.) was used without further purification.

Terahertz Spectroscopy

Terahertz time-domain spectra were recorded by a TAS7400TS THz-TDS (Advantest Co.). By using Fourier transformation, frequency-domain spectra in the region of 0.3-4 THz with frequency resolution of 7.6 GHz were obtained. The NaCl aqueous solutions were contained in a liquid cell made of polytetrafluoroethylene (PTFE), where a space with the thickness of 120 μm was inserted between the front and rear surfaces to keep the constant thickness of the liquid. The liquid cell was mounted at a copper holder inside of a cryostat (Janis ST-300, USA) to control the experimental conditions. The copper holder, with a 12-mm diameter empty circular aperture, was located at the terahertz beam's focal point to configure a transmission setup. Terahertz transparent diamond windows of the cryostat minimized unnecessary terahertz attenuation. An identical empty PTFE cell was also measured through the whole temperature range and the obtained spectra were used as the reference in calculation of the sample absorbance spectra. A full cooling-heating cycle to the NaCl solution was set to slowly cool from 296 K down to 223 K at a rate of 0.5 K every 3 min, and then heat to 296 K at the same rate. Similarly, 1 M KCl solution was also slowly frozen in the same way. The each terahertz spectrum was averaged over 256 scans to achieve the good signal-to-noise ratio; the total acquisition time of 256 scans lasts 30 s and the cryostat was set temperature unchanged during the spectra collection. The terahertz path was fully sealed and dry air was continuously purged to keep the humidity ≤1% to avoid the water absorption from atmosphere.

Low-Temperature X-Ray Diffraction

Low-temperature X-ray diffraction was performed using an 8D-ADVANCE X-ray diffractometer (λ = 1.5406 Å, tube voltage of 40 kV and tube current of 40 mA, Bruker Corporation, Germany) with a low-temperature chamber. The samples were scanned through 2ϑ range of 10-80°, with an angle step of 0.02°. The NaCl samples laid on the holder's surface of the diffractometer. The XRD patterns were measured at different temperatures.

Computational Method

Quantum chemical calculations based on solid-state density functional theory (DFT) were conducted to analyze and comprehend the measured terahertz spectra. The calculation was performed using Cambridge Sequential Total Energy Package (CASTEP) program,[32] a part of Materials Studio package from Accelrys. Perdew-Burke-Ernzerhof (PBE)[33] of generalized gradient approximation (GGA) was used as the exchange-correlation function, and Grimme's DFT-D2 dispersion-corrected method and norm-conserving pseudopotential were implemented in CASTEP.[34,35] In the calculations, the plane-wave cutoff energy was set as 830 eV and Brillouin zone sampling of electronic states was performed on a 2 × 1 × 2 Monkhorst-Pack grid. Vibrational frequencies and intensities of NaCl·$2H_2O$ molecules were obtained from Hessian matrix and atomic polar tensors respectively using the vibrational analysis tool packaged in the Materials Studio.

Results and discussion

The time-domain terahertz signals of 1 M NaCl sample in the heating and cooling cycles are presented in Figs. 1A and B, respectively. The peak amplitudes of the time-domain signals through the full cooling and heating cycles are plotted as a function of the temperature, as shown by black and red curves in Fig. 1C, respectively. Although the peak amplitude increases with cooling, there are three distinguishable segments shown clearly in the black curve: the linear increasing stage from 296 K to 263.5 K (phase I), nonlinear mutation stage down to 244 K (phase II), and saturation stage in temperature region of 244 to 223 K (phase III).

In the heating cycle, the mutation stage is noticeably shifted to higher temperatures comparing with that of cooling cycle. This shift, thermal hysteresis, is consentient with the first order phase transitions.[36] The thermal hysteresis has been studied experimentally in various systems including liquid crystals,[37] ferromagnetic single crystals,[38] and κ-carrageenan-water system.[39] In this study, the observed hysteresis could be originated from two factors: one is that the melting/crystallization processing lags behind the temperature variation during heating/cooling process; and the other is the

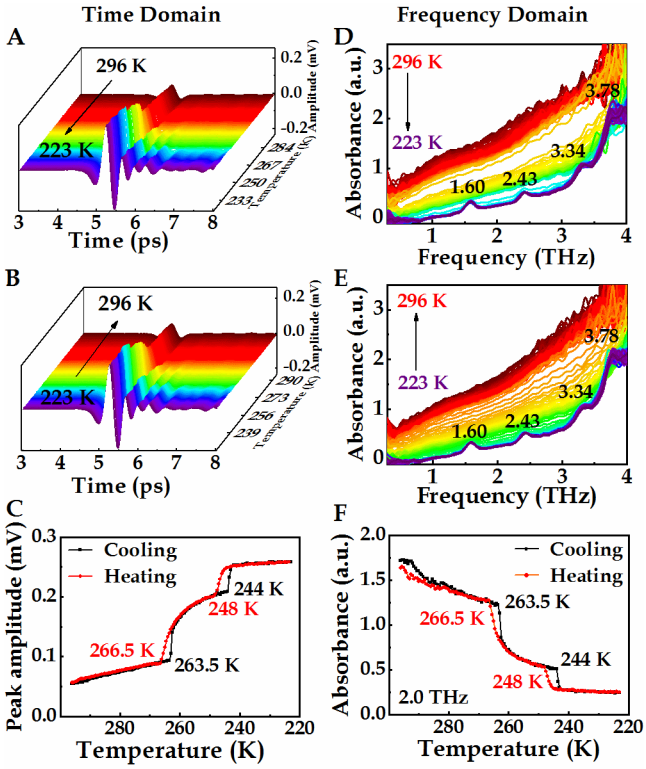

Fig. 1 Terahertz spectra of 1 M NaCl solution during cooling and heating processes in the temperature range of 223 to 296 K. A and B are the time domain THz signals at cooling (A) and heating (B) processes, and the corresponding absorbance in the frequency domain are shown in D and E, respectively. C and F are the temperature dependent hysteresis curves of electric field intensity in time domain and absorbance at 2.0 THz, respectively.

super-cooling effect in small-volume aqueous solutions. observed hysteresis. The frequency-domain terahertz absorbance obtained using Fourier transforming is presented in Figs. 1D and E in cooling and heating cycles, respectively. In both cooling and heating cycles, new absorption peaks appear at 1.60, 2.43, 3.34 and 3.78 THz at temperatures below 244 K. There are two possible reasons for the appearance of new absorption peaks at low temperatures. First, the echo signals within the hydrates layer of ions aggregated on the windows upon cooling might contribute to the observed peaks. Second, the low frequency vibrational mode of complex in the solution is highly responsible for the absorption. To exclude the echo effect, we performed the same experiment on 1 M KCl solution. If the absorption peaks in the NaCl solution were caused by the echo effect, similar peaks would also appear in the spectra of KCl solution. However, there is no absorption peak observed in KCl solution (see ESI.‡) and the echo effect can be excluded. Thus, these new peaks can only be caused by low frequency modes of the complex formed upon cooling.

The frequency-domain spectra of the NaCl solutions of 0, 0.3, 2.5 and 4.6 M are presented in Fig. 2 (more concentrations can see ESI.‡). The spectral profiles exhibit strong temperature and concentration dependence. The absorbance in the liquid phase at all concentrations, is relatively strong due to the dielectric relaxation of hydrogen bond networks and reorientation of the

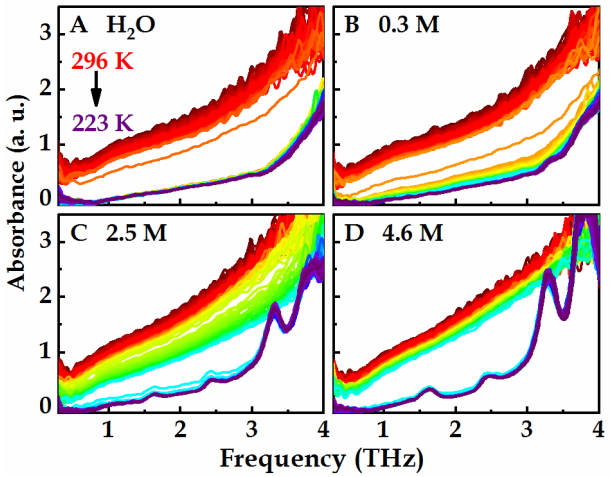

Fig. 2 Terahertz absorbance spectra of NaCl aqueous in the concentration range from 0 M to 4.6 M during the cooling process.

water molecular dipoles.[40] The absorbance at all concentrations decreases gradually with decreasing temperature until the liquid-solid phase transition temperatures. Below the liquid-solid phase transition temperatures, the absorbance decreases dramatically. The spectra profiles of NaCl solutions also exhibit strong concentration-dependent behaviours. For pure water, there is no identical feature observed at any measured temperatures in the studied terahertz frequency region. This observation is consistent with the previous report, which is mainly because of the broad distribution of hydrogen bond in water.[40] However, in NaCl solution at concentration of 0.3 M, the peak at 3.34 THz is obvious at temperatures below 243.5 K, while the peaks at lower frequencies are too weak to be observed. For samples with concentrations of 1 M, 2.5 M and 4.6 M, four distinct absorption peaks around 1.60 THz, 2.43 THz, 3.34 THz and 3.78 THz at temperatures lower than 243.5 K become obvious. Among them, the peaks centered at 3.34 THz and 3.78 THz are more pronounced at higher concentrations.

The absorbance at 2.0 THz for all NaCl samples are plotted as the function of cooling (black lines) and heating (red lines) cycles in Fig. 3. For pure water and NaCl solutions with concentration of 0.3 M, the absorbance in the cooling cycle first gradually decreases and drops dramatically at the freezing point of 268~266 K. This sudden change is caused by the formation of hexagonal (Ih) ice.[30] Similar sharp changes happen at the melting point of about 272~270.5 K in the heating cycle. Besides, there exists a stage of gradual increase of absorbance between the freezing and melting temperatures, which indicates partial melting of the samples.[19] The difference between heating and cooling cycle is due to the thermal hysteresis as mentioned above. It is worthy to clarify that because of the configuration of the setup, the thermometer settled on the sample holder is closer to liquid nitrogen, and thus the measured melting temperature of water 272 K is about 0.4% lower than 273.15 K.

For the samples with concentration between 0.2 M and 4.0 M, the freezing point decreases gradually with increasing the

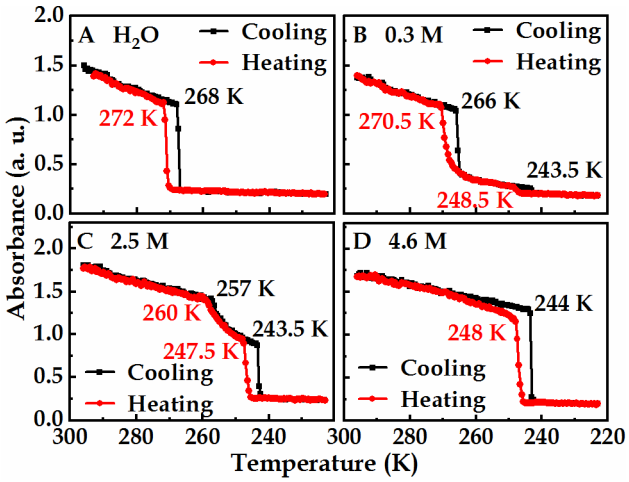

Fig. 3 The absorbance-temperature hysteresis curves derived from the absorbance amplitude at 2 THz. (A-D) correspond to different concentrations: 0, 0.3, 2.5 and 4.6 M.

concentrations, *i.e.*, from 266.5 K at 0.2 M to 246.5 K at 4.0 M during the cooling cycle (see ESI.‡). The second sharp change stage can be observed at the eutectic point of about 244 K. With increasing concentrations, the changes become more pronounced although the eutectic point remains stable. For the 4 M NaCl solution, a sharp change is observed at about 244 K in the cooling cycle, and around 248 K in the heating cycle. The observed freezing point and eutectic point indicate the phase separation of the ice, as well as the formation of new structures.

The concentration-dependent freezing temperature originates from the chemical potential which is correlated reciprocally with the concentration.[41,42] Increase of concentration of the solutions brought about decrease of the chemical potential, and thus reduce the freezing temperature. However, the eutectic point is independent on the concentration of NaCl solutions. This is because hydrated Na^+ and Cl^- ions were squeezed into a quasi-brine layer (QBL) and thus form saturated NaCl solution pools during freezing of the bulk water.[30,43,44] The concentration in saturated NaCl pools is a constant for all samples. This also explains why there is only one transition step in the saturated solution, as shown in Fig. 3D.

Figs. 4A and B depict the constructed temperature-concentration phase diagrams of NaCl aqueous solutions based on the THz measurements. Upon temperature decrease, the liquid phase (I) turns into solid ice phase (II), and now the hexagonal (Ih) ice and the saturated NaCl solution coexist. With further cooling, the NaCl hydrate is formulated (III), and then the hydrated NaCl crystals and the hexagonal (Ih) ices coexist together. For the cooling process, it can be seen that these three phases approach to a constant eutectic point around 4.6 M and 244 K. The phase diagrams of NaCl-H_2O obtained from THz-TDS data are fundamentally consistent with the conventional phase diagrams.[45]

In addition to the phase transition characterized by THz-TDS, the most striking observation is the appearance of four distinct absorption peaks at around 1.60, 2.43, 3.34 and 3.78 THz when the NaCl samples are frozen. As mentioned above, neither the ice nor the solid NaCl contributes to the terahertz absorption

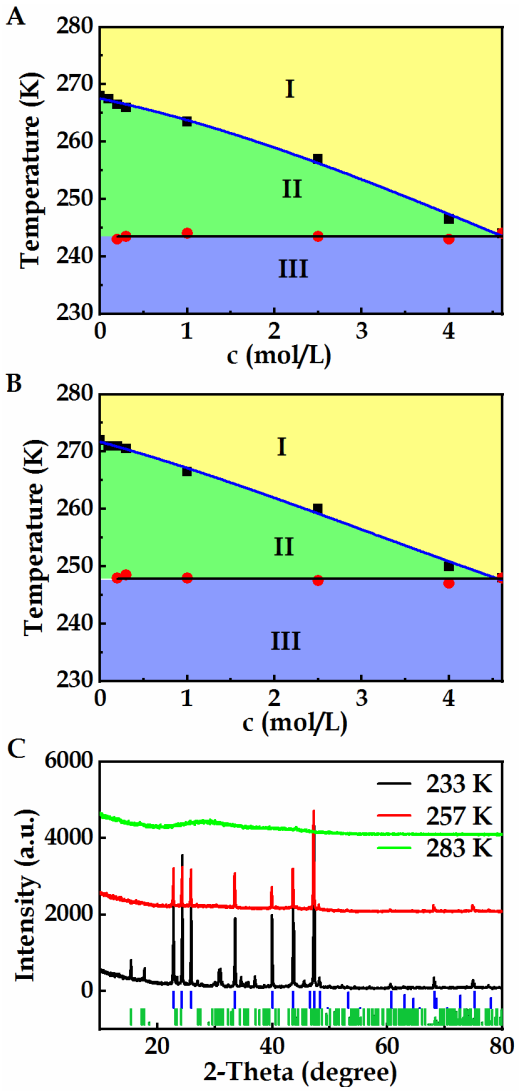

Fig. 4 Temperature-concentration phase diagram of NaCl aqueous solutions under the cooling (A) and heating (B) process; (C) The XRD patterns of 1 M NaCl solution at different temperatures. The vertical lines refer to standard pattern of the hexagonal ice (H_2O Ih PDF: 85-0857, blue) and NaCl·$2H_2O$ (PDF: 70-1158, green).

peaks below 4 THz,[46] and the emergence of new resonant absorption peaks is thus related to the hydrated NaCl. In fact, the hydrated NaCl crystal normally has a different crystal structure compared with the non-hydrated one, and thus displays different terahertz spectrum.[13] This is further confirmed by XRD measurements. Fig. 4C shows the measured XRD patterns for 1 M NaCl sample at the temperatures of 283 K, 257 K and 233 K. The vertical lines refer to standard pattern of hexagonal ice (H_2O Ih PDF: 85-0857, blue)[47] and NaCl hydrate (NaCl·$2H_2O$ PDF: 70-1158, green)[13]. The smooth (uniform) XRD pattern at 283 K indicates that the sample is in liquid stage, without crystallization forms. At T = 257 K, the observed sharp Bragg peaks originate from the scatterings of ice crystal, as the peaks match well with the pattern of Ih ice's diffraction diagrams (blue curves). While at T = 233 K, the observed XRD diagram contains patterns of both Ih ice and NaCl·$2H_2O$ hydrate, which indicates the coexistence of NaCl·$2H_2O$ hydrate and ice.

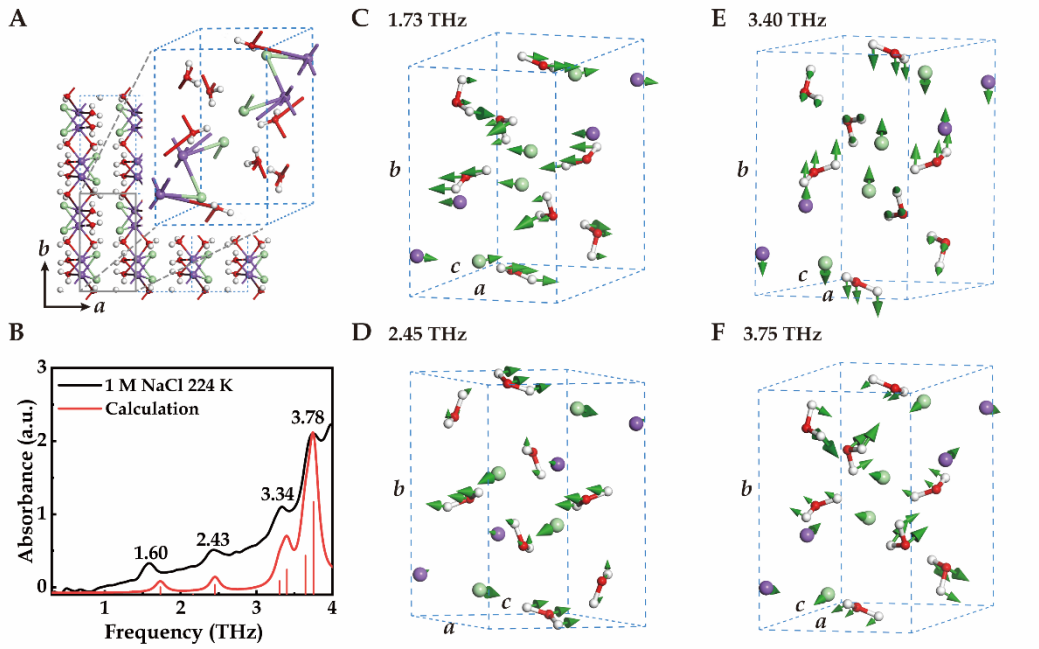

Fig. 5 The theoretical calculation results of THz spectroscopy and the corresponded vibrational modes of NaCl·2H_2O. (A) The crystal structure of NaCl·2H_2O viewed along the *c* axis, the enlarged frame shows a unit cell, and periodic boundary condition is employed in the calculation. The parameters of unit cell are a = 6.3313 Å, *b* = 10.1178 Å, *c* = 6.5029 Å, *β* = 114.4252°, *α* = *γ* = 90°.[13] Na^+ and Cl^- are represented by purple and green balls, respectively (B) The experimental and calculated THz spectra of NaCl·2H_2O. (C-F) The calculated vibrational modes of NaCl·2H_2O at (C) 1.73 THz, (D) 2.45 THz, (E) 3.40 THz and (F) 3.75 THz. Corresponding animations can be found in ESI.‡.

The XRD results are consistent with the phase diagrams presented in the Figs. 4A and B by the THz-TDS based spectroscopy analysis.

So far, all the evidence indicates that the newly emerged terahertz peaks observed in the phase III stage are ascribed to the formed hydrated NaCl crystal. For a complete understanding of these observed terahertz responses, quantum chemical calculations were performed using the CASTEP program. Fig. 5A shows the crystal structure of NaCl·2H_2O used in the calculation and the parameters of the NaCl·2H_2O crystal structure are *a* = 6.3313 Å, *b* = 10.1178 Å, *c* = 6.5029 Å, *β* = 114.4252°, *α* = *γ* = 90°.[13] The crystal structure is monoclinic with space group $P2_1/c$ (Z = 4).

Fig. 5B shows the simulated terahertz absorbance spectra and these distinctive absorption peaks are described as intermolecular vibrations.[48] For a clear view, the four vibrational modes of NaCl·2H_2O at 1.73, 2.45, 3.40 and 3.75 THz are demonstrated in Figs. 5C-F. Compared with the experimental conditions, the main difference of calculation is the setting of T = 0 K, which may slightly shift these peaks.[49,50] Except of the frequency shift, the calculation captured well with the terahertz experimental results. The vibrational mode at 1.73 THz, corresponding to the peak at 1.60 THz in the experimental spectra, arises from collective vibrations of all molecules in the unit cell, and the vibration directions lie mostly with the long diagonal of the *ac* plane. The peak at 2.45 THz, corresponding to the experimental peak at 2.43 THz, is assigned to the translational vibration of Na^+, Cl^- ions and parts of the water molecules along the short diagonal of the *ac* plane. The calculated feature at 3.40 THz is pointed to the measured peak at 3.34 THz, which primarily originates from the collective vibrations along b axis including Na^+, Cl^- ions and half of the water molecules. The calculated mode at 3.75 THz corresponds to the peak at 3.78 THz of the measured spectrum, and mainly comes from the collective vibrations along the long diagonal at an angle of about 45 degrees to the *ac* plane.

The results of DFT calculations further confirm that the newly discovered terahertz absorption peaks in the frozen NaCl solution are derived from the vibrational modes of NaCl·2H_2O crystal. The characterized features mainly originate from collective vibrations of molecules and each feature has been marked to a specific vibrational mode. Due to the symmetry and different locations of the molecules, the vibrational modes involve usually more than one type of movement due to molecules' spatial variation and structrural symmetries, therefore, these modes are expressed as diverse collective vibrations.

Conclusions

The NaCl hydrate formation from aqueous solutions was studied by THz-TDS over broad temperature and concentration ranges. The NaCl hydrate formation from aqueous solutions was accompanied with the remarkable phase transitions when freezing the solutions and the sensitive terahertz spectra could characterize both of them clearly. The formed NaCl hydrate gives rise to the emergence of new four collective vibrational modes at 1.60, 2.43, 3.34 and 3.78 THz and they could be ascribed to the vibrational modes of NaCl·2H_2O crystal, which can be further confirmed by the solid-state DFT calculations and

XRD measurements. The presented study demonstrated that the THz-TDS offers one simple and novel method to access the salt hydrate formations.

Conflicts of interest

There are no conflicts to declare.

Acknowledgements

This work was supported by the National Key Research and Development Program of China (with grant No. 2017YFA0701004), the National Science Foundation of China (Grant Nos. 61875150, 61935015, 61705163), the Tianjin Municipal Fund for Distinguished Young Scholars (18JCJQJC45600), and the National Defense Science and Technology Innovation Special Zone.

References

1 E. Gouaux and R. MacKinnon, *Science*, 2005, **310**, 1461-1465.
2 K. Ando and J. T. Hynes, *Adv. Chem. Phys.*, 1999, **6**, 381-430.
3 S. Koneshan, J. C. Rasaiah, R. M. Lynden-Bell and S. H. Lee, *J. Phys. Chem. B*, 1998, **102**, 4193-4204.
4 J. Israelachvili and H. Wennerström, *Nature*, 1996, **379**, 219-225.
5 R. W. Berg, *Appl. Spectrosc. Rev.*, 2018, **53**, 503-515.
6 P. Mazur, *Am. J. Physiol. Cell Physiol.*, 1984, **247**, C125-C142.
7 S. Bouazizi, S. Nasr, N. Jaîdane and M.-C. Bellissent-Funel, *J. Phys. Chem. B*, 2006, **110**, 23515-23523.
8 K. D. Collins, G. W. Neilson and J. E. Enderby, *Biophys. Chem.*, 2007, **128**, 95-104.
9 S. Bouazizi, F. Hammami, S. Nasr and M.-C. Bellissent-Funel, *J. Mol. Struct.*, 2008, **892**, 47-52.
10 Y. Kameda, Y. Amo, T. Usuki, Y. Umebayashi, K. Ikeda and T. Otomo, *Bull. Chem. Soc. Jpn.*, 2019, **92**, 754-767.
11 H. Cho, P. B. Shepson, L. A. Barrie, J. P. Cowin and R. Zaveri, *J. Phys. Chem. B*, 2002, **106**, 11226-11232.
12 R. Nanda, G. M. Bowers, N. Loganathan, S. D. Burton and R. J. Kirkpatrick, *RSC Adv.*, 2019, **9**, 12755-12765.
13 B. Klewe and B. Pedersen, *Acta Crystallogr., Sect. B: Struct. Crystallogr. Cryst. Chem.*, 1974, **30**, 2363-2371.
14 K. E. Håland and B. r. Pedersen, *J. Chem. Phys.*, 1973, **58**, 3472-3485.
15 Y. Gong, Y. Zhou, H. Wu, D. Wu, Y. Huang and C. Q. Sun, *J. Raman Spectrosc.*, 2016, **47**, 1351-1359.
16 D. Shin, J.-W. Lee, Y. Woo, M. Cha, Y. Lee, S. A. Chae, S. H. Kim, O. H. Han and J.-H. Yoon, *ACS Sustainable Chem. Eng.*, 2018, **6**, 5003-5010.
17 X. Chen, T. Yang, S. Kataoka and P. S. Cremer, *J. Am. Chem. Soc.*, 2007, **129**, 12272-12279.
18 E. Anim-Danso, Y. Zhang and A. Dhinojwala, *J. Am. Chem. Soc.*, 2013, **135**, 8496-8499.
19 Y. Zhang, E. Anim-Danso and A. Dhinojwala, *J. Am. Chem. Soc.*, 2014, **136**, 14811-14820.
20 L. Ho, M. Pepper and P. Taday, *Nat. Photonics*, 2008, **2**, 541-543.
21 A. I. McIntosh, B. Yang, S. M. Goldup, M. Watkinson and R. S. Donnan, *Chem. Soc. Rev.*, 2012, **41**, 2072-2082.
22 K. J. Tielrooij, N. Garcia-Araez, M. Bonn and H. J. Bakker, *Science*, 2010, **328**, 1006-1009.
23 P. Schienbein, G. Schwaab, H. Forbert, M. Havenith and D. Marx, *J. Phys. Chem. Lett.*, 2017, **8**, 2373-2380.
24 M. Śmiechowski, J. Sun, H. Forbert and D. Marx, *Phys. Chem. Chem. Phys.*, 2015, **17**, 8323-8329.
25 G. Schwaab, F. Sebastiani and M. Havenith, *Angew. Chem. Int. Ed.*, 2019, **58**, 3000-3013.
26 P. U. Jepsen and H. Merbold, *J. Infrared, Millimeter, Terahertz Waves*, 2010, **31**, 430-440.
27 Y. Marcus, *Chem. Rev.*, 2009, **109**, 1346-1370.
28 K. D. Collins, *Biophys. Chem.*, 2012, **167**, 43-59.
29 A. Shalit, S. Ahmed, J. Savolainen and P. Hamm, *Nat. Chem.*, 2017, **9**, 273-278.
30 K. Ajito, Y. Ueno, J.-Y. Kim and T. Sumikama, *J. Am. Chem. Soc.*, 2018, **140**, 13793-13797.
31 R. Rungsawang, Y. Ueno and K. Ajito, *Anal. Sci.*, 2007, **23**, 917-920.
32 J. Clark Stewart, D. Segall Matthew, J. Pickard Chris, J. Hasnip Phil, I. J. Probert Matt, K. Refson and C. Payne Mike, *Z. Kristallogr.*, 2005, **220**, 567-570.
33 J. P. Perdew, K. Burke and M. Ernzerhof, *Phys. Rev. Lett.*, 1996, **77**, 3865-3868.
34 S. Grimme, *J. Comput. Chem.*, 2006, **27**, 1787-1799.
35 Z. Xu, X. Lv, J. Chen, L. Jiang, Y. Lai and J. Li, *Carbon*, 2016, **107**, 885-894.
36 S. Yıldız, Ö. Pekcan, A. N. Berker and H. Özbek, *Phys. Rev. E*, 2004, **69**, 031705.
37 S. Sarmento, P. S. Carvalho, M. R. Chaves, F. Pinto and H. T. Nguyen, *Liq. Cryst.*, 2001, **28**, 1839-1845.
38 W.H. Wang, J.L. Chen, Z. Liu, G.H. Wu and W.S. Zhan, *Phys. Rev. B*, 2001, **65**, 012416.
39 S. Kara, C. Tamerler, H. Bermek and Ö. Pekcan, *J. Bioact. Compat. Polym.*, 2003, **18**, 33-44.
40 V. I. Gaiduk and D. S. F. Crothers, *J. Mol. Liq.*, 2006, **128**, 145-160.
41 V. I. Khvorostyanov and J. A. Curry, *J. Phys. Chem. A*, 2004, **108**, 11073-11085.
42 M. M. Conde, M. Rovere and P. Gallo, J. Mol. Liq., 2018, **261**, 513-519.
43 L. Vrbka and P. Jungwirth, *Phys. Rev. Lett.*, 2005, **95**, 148501.
44 T. Okada, *Chem. Rec.*, 2017, **17**, 415-428.
45 R. Cohen-Adad, P. Vallee and J. W. Lorimer, *Sodium chloride, in: R. Cohen-Adad, J.W. Lorimer (Eds.), Alkali metal and ammonium chlorides in water and heavy water (binary systems)*, Solubility Data Series; Pergamon Press: Oxford, U.K., 1991.
46 K. F. Pai, T. J. Parker, N. E. Tornberg, R. P. Lowndes and W. G. Chambers, *Infrared Physics*, 1978, **18**, 199-214.
47 L. G. Dowell and A. P. Rinfret, *Nature*, 1960, **188**, 1144-1148.
48 A. C. Jørgensen, C. J. Strachan, K. H. Pöllänen, V. Koradia, F. Tian and J. Rantanen, *J. Pharm. Sci.*, 2009, **98**, 3903-3932.
49 S. Baroni, S. de Gironcoli, A. Dal Corso and P. Giannozzi, *Rev. Mod. Phys*., 2001, **73**, 515-562.
50 Z. Zhu, C. Cheng, C. Chang, G. Ren, J. Zhang, Y. Peng, J. Han and H. Zhao, *Analyst*, 2019, **144**, 2504-2510.

